HHS Public Access

Author manuscript

Colloids Surf A Physicochem Eng Asp. Author manuscript; available in PMC 2017 August 20.

Published in final edited form as:

Colloids Surf A Physicochem Eng Asp. 2016 August 20; 503: 70–78. doi:10.1016/j.colsurfa.2016.05.038.

Molecular dynamics simulations on the effect of size and shape on the interactions between negative $Au_{18}(SR)_{14}$, $Au_{102}(SR)_{44}$ and $Au_{144}(SR)_{60}$ nanoparticles in physiological saline

Oscar D. Villareal[1,*], **Roberto A. Rodriguez**[1], **Lili Yu**[1,2], and **Thierry O. Wambo**[1]

[1]Department of Physics and Astronomy, University of Texas at San Antonio, San Antonio, Texas 78249, U.S.A

[2]Department of Laboratory Medicine, Yancheng Vocational Institute of Health Sciences, Jiangsu Yancheng 224006, P.R.C

Abstract

Molecular dynamics simulations employing all-atom force fields have become a reliable way to study binding interactions quantitatively for a wide range of systems. In this work, we employ two recently developed methods for the calculation of dissociation constants K_D between gold nanoparticles (AuNPs) of different sizes in a near-physiological environment through the potential of mean force (PMF) formalism: the method of geometrical restraints developed by Woo et al. and formalized by Gumbart et al. and the method of hybrid Steered Molecular Dynamics (hSMD). Obtaining identical results (within the margin of error) from both approaches on the negatively charged $Au_{18}(SR)_{14}$ NP, functionalized by the negatively charged 4-mercapto-benzoate (pMBA) ligand, we draw parallels between their energetic and entropic interactions. By applying the hSMD method on $Au_{102}(SR)_{44}$ and $Au_{144}(SR)_{60}$, both of them near-spherical in shape and functionalized by pMBA, we study the effects of size and shape on the binding interactions. Au_{18} binds weakly with $K_D = 13mM$ as a result of two opposing effects: its large surface curvature hindering the formation of salt bridges, and its large ligand density on preferential orientations favoring their formation. On the other hand, Au_{102} binds more strongly with $K_D = 30\mu M$ and Au_{144} binds the strongest with $K_D = 3.2nM$.

Keywords

Molecular Dynamics; Gold Nanoparticles; Aggregation

1. Introduction

The interactions in aqueous solutions of NPs with sizes less than 3 nm have recently become quantifiable through molecular dynamics (MD) simulations. [1, 2, 3, 4] Experimental studies

*Corresponding author: oscar.villarreal@utsa.edu (Oscar D. Villareal).

performed on large NPs (100 nm) have shown that aspherical shapes require a smaller salt concentration to aggregate, due to the larger contact areas between them;[5, 6] while smaller sizes require larger salt concentrations to aggregate, due to the weaker van der Waals forces of attraction.[7, 8] Such small-sized NPs have presented novel challenges to traditional colloid science theories such as Derjaguin-Landau-Verwey-Overbeak (DLVO). In particular, since the radius of sodium r_{Na} = 1.36 Å is more than 10% of the NP's radius, the Poisson-Boltzmann theory for electrostatic interactions is not reasonable because it considers the ions as point charges.[9] Additionally, the DLVO assumption that the surfaces of interaction are flat cannot be applied to NPs of such large curvatures as these.[10, 11] The presence of charged surface coatings also introduces steric and bridging effects (mediated by sodium) and it thus becomes necessary to replace simple analytic expressions by a PMF obtained from atomistic numerical computations.

In recent years, the computational methods for obtaining binding affinities through molecular dynamics simulations employing all-atom force fields have matured to a point that experimental measurements can be reproduced. In this paper, we illustrate the use of two such methods, both based on the *potentials of mean force* (PMF) formalism.[12, 13, 14] The first of these methods, which was developed in 2005 by Woo and Roux,[15] and whose procedures were formalized by Gumbart, Roux, and Chipot in 2012, "invokes a series of geometrical restraints acting on collective variables designed to alleviate sampling limitations inherent to classical molecular dynamics simulations."[16] The other method, which is called *hybrid Steered Molecular Dynamics* (hSMD)[17, 18], is a brute force approach developed in 2015 and involves mainly "simultaneously steering *n* centers of mass of *n* selected segments of the ligand using *n* springs of infinite stiffness".

In this work, we employ both methods on the $Au_{18}(SR)_{14}$ NP[19, 20, 21, 22] in a near-physiological environment (see Fig. 1(a)). Gold NPs have shown such a promising potential in medical procedures that the result has been called "a golden age" of biomedical nanotechnology.[23, 24] For example, they have been found suitable as drug delivery vehicles for selective targeting of cells,[25] as passive contrast agents for labelling, visualizing and tracking specific receptors,[26] as active sensors whose optical properties change in the presence of analyte molecules,[27] or as heat sources for the treatment of cancer through absorption of light.[28] With regard to biomedical applications, a desirable property of gold nanoparticles is their ability to aggregate reversibly into nanoclusters of controlled size when placed in a special solution, and to dissociate back into individual nanoparticles when introduced into the body.[29, 30, 31, 32] Finally, we compare the binding affinity of Au_{18} with those of Au_{102}[33] and Au_{144}[34, 35, 36, 37, 38, 39, 40, 32], functionalized by the same ligand under the same near-physiological conditions.

2. Methods

Simulation Parameters

All interactions were represented with the CHARMM36 force field.[42] Water was represented with the TIP3P[43] model. The cut-off distance applied to the vdW interactions was 1.2 nm, with a switching distance of 1.0 nm and a pair list distance of 1.35 nm. Langevin dynamics were implemented with a time-step of 1.0 fs for short range interactions

and 2.0 fs for long range interactions, and with a Langevin damping of 1.0 ps^{-1}. The temperature was kept at 298 K and the pressure at 1.0 bar using the Nose-Hoover Langevin piston control.[44, 45] Periodic boundary conditions were applied in all dimensions. Full electrostatic interactions were computed through the Particle-Mesh Ewald (PME) method. All simulations were performed with NAMD.[46]

Building procedure for the AuNP

The coordinates of the $Au_{18}S_{14}$ and $Au_{102}S_{44}$ cores were obtained in Refs. [19] and [33] respectively. We chose the negatively charged 4-mercapto-benzoate ligand because of its experimental relevance. [47, 48] We bound a copy of this ligand to each sulfur and minimized the resulting structure in vacuum while fixing the core atoms (see Video 1 in the Supplementary data). The distances between each gold atom were restrained to their initial values in order to make the core rigid, while still allowing it to move freely. A copy of the NP was then placed 4 nm apart. Since $Au_{18}S_{14}$ is non-spherical, we determined the orientation of strongest attraction by placing 16 sodium ions in the plane at the middle and allowing the NPs to rotate freely in vacuum (see Fig. 2(b)). After removing the ions at the middle, the NPs were placed in a 70x70x140 $Å^3$ water box with a 150 mM concentration of NaCl. The system comprised a total of 64 964 atoms.

Computing binding affinities from potentials of mean force

Following the standard literature,[15] the dissociation constant K_D for the process of binding between two rigid NPs can be computed through the potential of mean force $\mathscr{W}(\mathbf{r})$ formalism as:

$$\frac{c_0}{K_D} = c_0 e^{-\beta \Delta G_{\text{bind}}} = \frac{c_0 \int_{\text{site}} d\mathbf{r} e^{-\beta \mathscr{W}(\mathbf{r})}}{\int_{\text{bulk}} d\mathbf{r} \delta(\mathbf{r} - \mathbf{r}_\infty) e^{-\beta \mathscr{W}(\mathbf{r})}} \quad (1)$$

where the sampling in the numerator of Eq. (1) is performed on the ensemble of microstates belonging to the bound state, while the sampling in the denominator is performed on the ensemble of microstates from the unbound state. $\mathbf{r}_\infty$ is defined to be any microstate belonging to the unbound state, $\beta = 1/k_B T$, c_0 is the concentration at standard conditions, equal to 1M on the left-hand side of the equation, and $\frac{6.02 \times 10^{23}\ \text{nanoparticles}}{10^{27} Å^3}$ on the right-hand side. Further details are presented in the supplementary information (SI), section 1.

The hSMD method

If we define $\mathbf{r}_0$ to be one of the states from the ensemble of bound states, $\mathbf{r}_\infty$ to be one of the states from the ensemble of unbound states, and the free-energy difference between these two states to be $\Delta \mathscr{W}_{0,\infty} \equiv \mathscr{W}(\mathbf{r}_0) - \mathscr{W}(\mathbf{r}_\infty)$, then, as in Ref. [17], we have

$$\Delta G_{\text{bind}} = \Delta \mathscr{W}_{0,\infty} - k_B T \ln\left(\frac{c_0 Z_0}{Z_\infty}\right) \quad (2)$$

where $Z_0 \equiv \int_{\text{site}} d\mathbf{r} e^{-\beta[\mathscr{W}(\mathbf{r})-\mathscr{W}(\mathbf{r}_0)]}$ and $Z_\infty \equiv \int_{\text{bulk}} d\mathbf{r} e^{-\beta[\mathscr{W}(\mathbf{r})-\mathscr{W}(\mathbf{r}_\infty)]}$ correspond to sampling over the ensembles of bound states and unbound states, respectively, and constitute the entropic contribution to the binding affinity. The scheme of simulations employed to drag the system along the dissociation path from $\mathbf{r}_0$ to $\mathbf{r}_\infty$ is presented in the SI, Fig. S1.

The hSMD method applied to the Au_{18} NP

The energetic interactions were studied by selecting arbitrarily three atoms ($\mathbf{r}_1$, $\mathbf{r}_2$, $\mathbf{r}_3$) at the center of the NP whose core was not fixed and pulling them individually along straight lines relative to the NP whose core was fixed until the NPs became aggregated. In this way, the one-dimensional PMF as function of center-to-center distance was obtained, and the NPs were not allowed to rotate at this stage. In order to study the entropic interactions, we performed two runs of 20 ns each under equilibrium conditions: one in which the NPs were bound, and another in which they were unbound. During the bound-state simulation, the core of one NP was fixed while the other NP moved freely (see Video 2 in the Supplementary data) and Z_0 was approximated as a Gaussian integration:

$$Z_0 = \sqrt{(2\pi)^9 |\sum|} \quad e^{\frac{1}{2}(\mathbf{r}_1,\mathbf{r}_2,\mathbf{r}_3)\bullet\sum^{-1}\bullet(\mathbf{r}_1,\mathbf{r}_2,\mathbf{r}_3)^T} \quad (3)$$

where Σ is the matrix containing the variances of the coordinates in time:

$$\sum = \begin{bmatrix} \langle\delta x_1^2\rangle & \langle\delta x_1\delta y_1\rangle & \langle\delta x_1\delta z_1\rangle & \dots & \langle\delta x_1\delta x_3\rangle & \langle\delta x_1\delta y_3\rangle & \langle\delta x_1\delta z_3\rangle \\ \langle\delta y_1\delta x_1\rangle & \langle\delta y_1^2\rangle & \langle\delta y_1\delta z_1\rangle & \dots & \langle\delta y_1\delta x_3\rangle & \langle\delta y_1\delta y_3\rangle & \langle\delta y_1\delta z_3\rangle \\ \langle\delta z_1\delta x_1\rangle & \langle\delta z_1\delta y_1\rangle & \langle\delta z_1^2\rangle & \dots & \langle\delta z_1\delta x_3\rangle & \langle\delta z_1\delta y_3\rangle & \langle\delta z_1\delta z_3\rangle \\ \vdots & \vdots & \vdots & \ddots & \vdots & \vdots & \vdots \\ \langle\delta x_3\delta x_1\rangle & \langle\delta x_3\delta y_1\rangle & \langle\delta x_3\delta z_1\rangle & \dots & \langle\delta x_3^2\rangle & \langle\delta x_3\delta y_3\rangle & \langle\delta x_3\delta z_3\rangle \\ \langle\delta y_3\delta x_1\rangle & \langle\delta y_3\delta y_1\rangle & \langle\delta y_3\delta z_1\rangle & \dots & \langle\delta y_3\delta x_3\rangle & \langle\delta y_3^2\rangle & \langle\delta y_3\delta z_3\rangle \\ \langle\delta z_3\delta x_1\rangle & \langle\delta z_3\delta y_1\rangle & \langle\delta z_3\delta z_1\rangle & \dots & \langle\delta z_3\delta x_3\rangle & \langle\delta z_3\delta y_3\rangle & \langle\delta z_3^2\rangle \end{bmatrix} \quad (4)$$

This approximation is valid when the binding is tight. Since the Au_{18} NPs are non-spherical, their binding is tight only when their orientations correspond to the maximum contact area between them, that is, to a maximum formation of salt bridges. Because of this, we would not expect the NPs to roll on top of each other, but rather to remain in the initial binding orientation (the Euler angles of the free NP are plotted in Fig. 6(b)).

During the unbound-state simulation, only one NP was employed. Z_∞ was obtained by sampling over the coordinates of groups 2 and 3 while keeping group 1 fixed:

$$Z_\infty = \int_{bulk} d\mathbf{r}_2 d\mathbf{r}_3 e^{-\beta[\mathscr{W}(\mathbf{r}_{1\infty},\mathbf{r}_2,\mathbf{r}_3)-\mathscr{W}(\mathbf{r}_{1\infty},\mathbf{r}_{2\infty},\mathbf{r}_{3\infty})]} = \int_{\text{bulk}} d\mathbf{r}_3 e^{-\beta[\mathscr{W}(\mathbf{r}_{1\infty},\mathbf{r}_{2\infty},\mathbf{r}_3)-\mathscr{W}(\mathbf{r}_{1\infty},\mathbf{r}_{2\infty},\mathbf{r}_{3\infty})]} \times \int_{\text{bulk}} d\mathbf{r}_2 e^{-\beta[\mathscr{W}(\mathbf{r}_{1\infty},\mathbf{r}_2)-\mathscr{W}(\mathbf{r}_{1\infty},\mathbf{r}_{2\infty})]} \quad (5)$$

The first term of equation 5 is obtained by sampling over the distance r_{23} between groups 2 and 3, as well as over the angle θ formed by the three groups. This corresponds to placing group 2 at the origin and group 1 at the z axis. r_{23}, θ, φ are then the spherical coordinates of group 3, where φ is integrated out. In the second term of equation 5 we can then integrate out θ and φ, and sample over the distance r_{12} between groups 1 and 2. These integrations are also made through the Gaussian approximation:

$$Z_\infty \approx \left[2\pi r_{23\infty}^2 \sin\theta_\infty \sqrt{(2\pi)^2 |r_{23},\theta|} e^{\frac{1}{2}(r_{23},\theta)\bullet\sum_{(r_{23},\theta)}^{-1}\bullet(r_{23},\theta)^T}\right] \times \left[4\pi r_{12\infty}^2 \sqrt{2\pi|\sum_{r_{12}}|} e^{\frac{1}{2}r_{12}\bullet\sum_{r_{12}}^{-1}\bullet r_{12}}\right] \quad (6)$$

where $r_{12\infty}$, $r_{23\infty}$ and θ_∞ are the average values of the simulation, $\sum_{(r_{23},\theta)} = \begin{bmatrix} \langle\delta r_{23}^2\rangle & \langle\delta r_{23}\delta\theta\rangle \\ \langle\delta r_{23}\delta\theta\rangle & \langle\delta\theta^2\rangle \end{bmatrix}$ and $\sum_{r_{12}} = \langle\delta r_{12}^2\rangle$ (more details are presented in the SI, section 2).

The hSMD method applied to the Au_{102} and Au_{144} NPs

Since these NPs are near-spherical, the PMF is independent of the Euler angles defining their orientation, as well as of the angular spherical coordinates defining their angular position. The PMF is a one-dimensional function of the radial separation between the NPs: [49]

$$\frac{c_0}{K_D} = c_0 \int_{site} d\mathbf{r} e^{-\beta\mathscr{W}(\mathbf{r})} = 4\pi c_0 \int_0^{r^*} r^2 dr\, e^{-\beta\mathscr{W}(r)} \quad (7)$$

where r^* is a reference position far away in the bulk (i.e. at the dissociated state, where $\mathscr{W}(r) \rightarrow 0$ by definition). In the case of the Au_{102} NP, we pulled the center of mass of the 7 gold atoms located at the center, considered as a single atomic group. In this way, we allowed the particle to rotate freely during the dissociation. As for the Au_{144} NP, we chose the 12 gold atoms at the center which form an icosahedron, and the same procedure was followed (see the SI, section 3 for additional details).

The method of geometrical restraints

Following Ref. [16], three atomic groups are defined on each of the binding partners. Six collective variables are then defined in terms of these groups: three Euler angles (Θ, Φ, Ψ) specifying the orientation of the body, and three spherical coordinates specifying its position

(θ, φ, r), where r is the separation between the partners. A seventh collective variable is the body's conformation, expressed by its root-mean-square deviation (RMSD) with respect to its time-averaged structure at the bound state. These variables each represent a component of the dissociation path. The free energy of binding is given by:

$$\Delta G_{\text{bind}} = -G_c^{\text{site}} - G_0^{\text{site}} - G_a^{\text{site}} - k_B T \ln(c_0 S^* I^*) + G_c^{\text{bulk}} + G_0^{\text{bulk}} \quad (8)$$

where $I^* \equiv \int_{\text{site}} d\mathbf{r} e^{-\beta[\mathcal{W}(\mathbf{r}) - \mathcal{W}(\mathbf{r}_\infty)]}$ and $S^* \equiv (\mathbf{r}_\infty)^2 \int_0^\pi d\theta \sin\theta \int_0^{2\pi} d\phi e^{-\beta u_a}$ correspond to the positional contributions to the free energy as the object is dragged away from the binding site; G_c^{site} and G_c^{bulk} correspond to the contributions of the RMSD degree of freedom at the site and the bulk regions, respectively; G_0^{site} and G_0^{bulk} correspond to the orientational degrees of freedom, and G_a^{site} corresponds to the two spherical angles at the bound state (the term G_a^{bulk} is implicit in the $S^* I^*$ product). Further specifics of this methodology are presented in the SI, section 5.

The method of geometrical restraints applied to the Au_{18} NP

Since the shape of the Au_{18} NP is non-spherical, sampling over its orientational degrees of freedom becomes necessary. We defined three groups of atoms on the NP whose core was fixed, and three on the other NP. In Fig. 3(a), as well as in Video 3 in the Supplementary data, we present the collective variables defining both the orientation and the location of the free $Au_{18}(SR)_{14}$ NP relative to the fixed one.

3. Results

From the hSMD method

In Fig. 4(a) we plot the location over time of the three pulling atoms during a bound-state equilibration. Fig. 4(b) shows the separations among the atoms and the angle made by them during an unbound-state equilibration. From this sampling we obtained the entropic contributions to the K_D of Au_{18}, shown in Table 1. In Fig. 4(c) we show the PMF for the dissociation and compare it to those of Au_{102} and Au_{144}(the results for Au_{144} were taken from Ref. [40]). Through these PMFs we obtained the energetic contributions to K_D. These simulations are presented in Videos 4, 5 and 6 in the Supplementary data. The PMFs were obtained from the work profiles shown in the SI, Fig. S4. As shown in Fig.4(d), the smaller the NP was, the weaker the van der Waals attraction became. The non-spherical shape of Au_{18} originated the non-isotropic distribution of ligands and ions shown in Fig. 5(a). During the bound-state simulation, five sodium were observed to lie on average at the region in-between the two Au_{18} and forming salt-bridges between them. As for Au_{102} and Au_{144}, we found on average eight and eleven salt-bridges in their bound states, respectively (see Figs. 5(b),(c)). The average number of salt bridges was estimated by counting the amount of ions lying within 0.35nm of both nanoparticles simultaneously (this value was taken from ref. [35] as the cutoff distance of contact between an ion and a terminal group).

From the method of geometrical restraints

In Figs. 6(a),(b),(c) we plot the collective variables as functions of time during a run under equilibrium conditions as it was bound to another Au_{18} whose core's location was fixed. Figs. 6(d),(e),(f) show the PMFs as functions of the collective variables. In Table 1 we present the contributions to the free energy from each collective variable, which resulted in a dissociation constant of ≈ 9.0 mM.

Spontaneity of the aggregation

We performed a simulation under equilibrium conditions of a pair of free Au_{18} NPs in order to verify the spontaneity of their aggregation, in the absence of external forces or constraints. The initial center-to-center distance was set at 3 nm, since at this point the PMF of Fig. 4(c) starts becoming attractive. The center-to-center distance is plotted vs. time in Fig. 7(a) and the simulation is shown in Video 7 of the supplementary data. Notice how the separation between the NPs decreases to the value corresponding to the minimum in the PMF within the first 5 ns, and it remains stable for the next 15 ns.

Specificity of the binding site

In the case of the Au_{144} and Au_{102} NPs, due to their spherical shape the binding site could lie anywhere at the surface. Thanks to this their dissociation constant can be obtained from eq. 7 without the need to sample over their bound and unbound states. A one-dimensional PMF as function of separation between the NPs connecting one of the bound states to one of the dissociated states contains implicitly the sampling over the full surface area of the sphere.[49] However, in the case of the Au_{18}, their non-spherical shape causes the binding site to become specific to those orientations which allow for the formation of a maximum amount of salt bridges. In order to verify this, we measured an additional PMF using the opposite orientation from that employed in Fig. 4. The PMF profile of Fig. 7(b) became repulsive and thus no binding was observed.

4. Discussion

The aggregation process of Au_{18} NPs

In the SI, Fig. S2(a), we see that as the NPs approach, the direct electrostatic repulsion between them appears much sooner than the van der Waals attraction, which is weak when compared with the PMF. As the NPs approach, the electrostatic energy between them and the sodium ions decreases (see the SI, Fig. S2(b)), since the sodium is able to form salt bridges between the two NPs. However, as the sodium ions transition from being bound with one ligand to being bound with two ligands, they have to be partially dehydrated. This repulsive interaction opposes the decrease in the ion-NP electrostatic energy. Such hydration repulsion is a general property of hydrophilic surfaces.[50, 51, 52] An additional repulsive interaction of the binding process is the decrease in entropy of both the sodium ions and the ligands as their motion becomes more restricted during the formation of the salt bridges. We may observe from the method of geometrical restraints that the entropic contributions to the free energy were: $\Delta G_c^{\mathrm{bulk}} + \Delta G_c^{\mathrm{site}} = 2\,\mathrm{kcal/mol}$ for the conformational component, $\Delta G_o^{\mathrm{bulk}} + \Delta G_\Theta^{\mathrm{site}} + \Delta G_\Phi^{\mathrm{site}} + \Delta G_\Psi^{\mathrm{site}} = 0.8\,\mathrm{kcal/mol}$ for the rotational component and

$\Delta G_{\theta}^{\mathrm{site}}+\Delta G_{\phi}^{\mathrm{site}}-k_{B}T\ln\left(c_{0}S^{*}I^{*}\right)=5.6\,\mathrm{kcal/mol}$ for the translational component. Both the conformational and rotational components favor the unbound states, where the entropic freedom is larger. However, the translational component (which favors the bound state) is larger than the other two combined.

Size and Shape effects of AuNPs

Because of the small size of the Au_{18} NP (≈ 1 nm for the core diameter) the resulting large curvature decreases the contact area between two such NPs, thus hindering the formation of salt bridges between them. The small size also decreases the strength of the van der Waals attraction. On the other hand, the non-spherical shape of this NP increases the contact area on those sides whose curvatures are smaller, thus facilitating the formation of salt bridges at preferential orientations. Yet by limiting the orientations which are available for binding, an entropic repulsion is also originated, since there is a decrease in the amount of bound states. In Fig. 7 we saw that for some orientations the interaction actually becomes repulsive. Because of these reasons, as shown in Fig. 4(h), when we compare the PMF of Au_{18} with those of Au_{102} and Au_{144} (functionalized by the same ligand and in the same near-physiological conditions), the attraction between the Au_{18} NPs was observed to be the weakest, while that of Au_{144} was the strongest. This result agrees with recent experimental data from ultrasmall glutathione-coated gold nanoparticles.[53] The minima in the PMF profiles of the three NPs studied in this work was found to decrease linearly with the size:

$$\mathscr{W}_{min}\sim 1-6\times D \quad (9)$$

where D is the diameter of the NP in units of nm.

Application of the methods on the Ligand-Protein problem

In the supplementary data we show the results from both methods on a protein-ligand binding process with known experimental value of dissociation constant: the acetazolamide (AZM) drug bound to the aquaporin 4 (AQP4) water-channel protein (see Video 8 of the Supplementary data). AZM has been found to inhibit water permeation through AQP4 with an IC_{50} of ≈ 3 mM.[54] Identical results (within the margin of error) were obtained from both approaches, in agreement with experimental measurements.

5. Conclusion

In this work, we compared the interactions of Au_{18}, Au_{102} and Au_{144}, all three functionalized by the same $SPh(COO^{-})$ ligand under the same near-physiological saline conditions. On the one hand, the smaller size of the Au_{18} hinders the formation of salt bridges between two NPs because of its larger curvature and thus smaller contact area. At the same time, its smaller size decreases the strength of the van der Waals attraction. On the other hand, the non-isotropic shape of Au_{18} facilitates the formation of salt bridges by increasing the contact area on preferential orientations; yet it also increases the entropy of the bound state by limiting the orientations available for binding. This resulted in dissociation constants of 13mM, 30μM and 3.2nM for Au_{18}, Au_{102} and Au_{144} respectively.

The results for Au_{18} from two different methods agreed with each other. We therefore expect our results to be confirmed in future experiments.

We employed two computational methods for the calculation of absolute binding free energies from the PMF. The method of geometrical restraints is able to separate the contributions to the free energy into nine different geometrical components, in this way providing a great amount of detail regarding the origins of the result. The hSMD method is able to compute the free energy in a brute-force way without losing accuracy, in this way saving much effort during its implementation. Depending on the system under consideration, one may be interested in maximizing the output of information through the use of a series of biasing and constraining potentials, or in computing the result in a straightforward way through the use of steering/pulling simulations. Both methods provide a complete atomic-level picture of the interactions which lie at the origin of the result.

Supplementary Material

Refer to Web version on PubMed Central for supplementary material.

Acknowledgments

The authors acknowledge support from the NIH (GM 084834) and the computing resources provided by the Texas Advanced Computing Center at University of Texas at Austin. ODV acknowledges a graduate scholarship from the Mexican National Council of Science and Technology (CONACYT Grant 533262). LY acknowledges the Jiangsu Overseas Research & Training Program for University Prominent Young & Middle-aged Teachers and Presidents. Finally, the authors would like to express their gratitude to Dr. Liao Y. Chen for his continued guidance and support in their research endeavors.

References

1. Jabes BS, Yadav HOS, Kumar SK, Chakravarty C. Fluctuation-driven anisotropy in effective pair interactions between nanoparticles: Thiolated gold nanoparticles in ethane. J Chem Phys. 2014; 141(15):154904. doi:doi:http://dx.doi.org/10.1063/1.4897541. [PubMed: 25338910]
2. Sun L, Yang X, Wu B, Tang L. Molecular simulation of interaction between passivated gold nanoparticles in supercritical co2. J Chem Phys. 2011; 135(20):204703. doi:doi:http://dx.doi.org/10.1063/1.3661982. [PubMed: 22128948]
3. Patel N, Egorov SA. Interactions between sterically stabilized nanoparticles in supercritical fluids: A simulation study. J Chem Phys. 2007; 126(5):054706. doi:doi:http://dx.doi.org/10.1063/1.2434155. [PubMed: 17302497]
4. Heikkil E, Martinez-Seara H, Gurtovenko AA, Javanainen M, Hkkinen H, Vattulainen I, Akola J. Cationic au nanoparticle binding with plasma membrane-like lipid bilayers: Potential mechanism for spontaneous permeation to cells revealed by atomistic simulations. The Journal of Physical Chemistry C. 2014; 118(20):11131–11141. arXiv: http://dx.doi.org/10.1021/jp5024026. DOI: 10.1021/jp5024026
5. Guo Z, Fan X, Xu L, Lu X, Gu C, Bian Z, Gu N, Zhang J, Yang D. Shape separation of colloidal gold nanoparticles through salt-triggered selective precipitation. Chem Commun. 2011; 47(14): 4180–4182. DOI: 10.1039/C0CC04612D
6. Hao M, Liu C, Peng L, Li J, Lu W, Jiang L. Shape separation of gold nanoparticles using a ph-responsive amphiphilic dendrimer according to their shape anisotropy distinction. J Colloid Interface Sci. 2015; 437:311–315. doi:http://dx.doi.org/10.1016/j.jcis.2014.09.052. [PubMed: 25441366]
7. Zhao W, Lin L, Hsing IM. Nucleotide-mediated size fractionation of gold nanoparticles in aqueous solutions. Langmuir. 2010; 26(10):7405–7409. DOI: 10.1021/la9044489 [PubMed: 20180584]

8. Yang H, Heng X, Wang W, Hu J, Xu W. Salt-induced size-selective separation, concentration, and preservation of zwitterion-modified gold nanoparticles. RSC Advances. 2012; 2(7):2671–2674. DOI: 10.1039/C2RA00828A
9. Silvera Batista CA, Larson RG, Kotov NA. Nonadditivity of nanoparticle interactions. Science. 350(6257) arXiv: http://www.sciencemag.org/content/350/6257/1242477.full.pdf.
10. Hotze EM, Phenrat T, Lowry GV. Nanoparticle aggregation: challenges to understanding transport and reactivity in the environment. J Environ Qual. 2010; 39(6):1909–24. DOI: 10.2134/jeq2009.0462 [PubMed: 21284288]
11. Delgado AV, Gonzlez-Caballero F, Hunter RJ, Koopal LK, Lyklema J. IU of Pure, P Applied Chemistry, BCDIT Report. Measurement and interpretation of electrokinetic phenomena. J Colloid Interface Sci. 2007; 309(2):194–224. DOI: 10.1016/j.jcis.2006.12.075 [PubMed: 17368660]
12. Kirkwood JG. Statistical mechanics of fluid mixtures. J Chem Phys. 1935; 3(5):300–313. DOI: 10.1063/1.1749657
13. Allen TW, Andersen OS, Roux B. Molecular dynamics - potential of mean force calculations as a tool for understanding ion permeation and selectivity in narrow channels. Biophys Chem. 2006; 124(3):251–67. DOI: 10.1016/j.bpc.2006.04.015 [PubMed: 16781050]
14. Roux B. The calculation of the potential of mean force using computer-simulations. Comput Phys Commun. 1995; 91(1–3):275–282. DOI: 10.1016/0010-4655(95)00053-I
15. Woo HJ, Roux B. Calculation of absolute protein-ligand binding free energy from computer simulations. Proc Natl Acad Sci U S A. 2005; 102(19):6825–30. DOI: 10.1073/pnas.0409005102 [PubMed: 15867154]
16. Gumbart JC, Roux B, Chipot C. Standard binding free energies from computer simulations: What is the best strategy? J Chem Theory Comput. 2012; 9(1):794–802. DOI: 10.1021/ct3008099 [PubMed: 23794960]
17. Chen LY. Hybrid steered molecular dynamics approach to computing absolute binding free energy of ligand-protein complexes: A brute force approach that is fast and accurate. J Chem Theory Comput. 2015; 11(4):1928–1938. DOI: 10.1021/ct501162f [PubMed: 25937822]
18. Rodriguez RA, Yu LL, Chen LY. Computing protein-protein association affinity with hybrid steered molecular dynamics. J Chem Theory Comput. 2015; 11(9):4427–4438. DOI: 10.1021/acs.jctc.5b00340 [PubMed: 26366131]
19. Tlahuice A, Garzón IL. On the structure of the au18(sr)14 cluster. Phys Chem Chem Phys. 2012; 14(11):3737.doi: 10.1039/c2cp24016e [PubMed: 22323014]
20. Das A, Liu C, Byun HY, Nobusada K, Zhao S, Rosi N, Jin R. Structure determination of [au18(sr)14]. Angewandte Chemie. 2015; 127(10):3183–3187. DOI: 10.1002/ange.201410161
21. Reilly SM, Krick T, Dass A. Surfactant-free synthesis of ultrasmall gold nanoclusters. J Chem Phys C. 2010; 114(2):741–745. DOI: 10.1021/jp9067944
22. Jiang, D-e; Chen, W.; Whetten, RL.; Chen, Z. What protects the core when the thiolated au cluster is extremely small? J Chem Phys C. 2009; 113(39):16983–16987. DOI: 10.1021/jp906823d
23. Dreaden EC, Alkilany AM, Huang X, Murphy CJ, El-Sayed MA. The golden age: gold nanoparticles for biomedicine. Chem Soc Rev. 2012; 41(7):2740–2779. DOI: 10.1039/C1CS15237H [PubMed: 22109657]
24. Sperling RA, Rivera Gil P, Zhang F, Zanella M, Parak WJ. Biological applications of gold nanoparticles. Chem Soc Rev. 2008; 37(9):1896–1908. DOI: 10.1039/B712170A [PubMed: 18762838]
25. Grace AN, Pandian K. Antibacterial efficacy of aminoglycosidic antibiotics protected gold nanoparticlesa brief study. Colloids Surf A: Physicochem Eng Aspects. 2007; 297(13):63–70. doi:http://dx.doi.org/10.1016/j.colsurfa.2006.10.024.
26. Tang F, Wang C, Wang X, Li L. Preparation of biocompatible fluorescent coreshell nanoparticles for cellular imaging. Colloids Surf A: Physicochem Eng Aspects. 2015; 485:49–54. doi:http://dx.doi.org/10.1016/j.colsurfa.2015.09.010.
27. Wang X, Wei Y, Wang S, Chen L. Red-to-blue colorimetric detection of chromium via cr (iii)-citrate chelating based on tween 20-stabilized gold nanoparticles. Colloids Surf A: Physicochem Eng Aspects. 2015; 472:57–62. doi:http://dx.doi.org/10.1016/j.colsurfa.2015.02.033.

28. Oni Y, Hao K, Dozie-Nwachukwu S, Obayemi JD, Odusanya OS, Anuku N, Soboyejo WO. Gold nanoparticles for cancer detection and treatment: The role of adhesion. J Appl Phys. 2014; 115(8): 084305. doi:doi:http://dx.doi.org/10.1063/1.4863541.
29. Murthy AK, Stover RJ, Borwankar AU, Nie GD, Gourisankar S, Truskett TM, Sokolov KV, Johnston KP. Equilibrium gold nanoclusters quenched with biodegradable polymers. ACS Nano. 2013; 7(1):239–251. arXiv:http://dx.doi.org/10.1021/nn303937k. DOI: 10.1021/nn303937k [PubMed: 23230905]
30. Murthy AK, Stover RJ, Hardin WG, Schramm R, Nie GD, Gourisankar S, Truskett TM, Sokolov KV, Johnston KP. Charged gold nanoparticles with essentially zero serum protein adsorption in undiluted fetal bovine serum. J Am Chem Soc. 2013; 135(21):7799–7802. arXiv:http://dx.doi.org/10.1021/ja400701c. DOI: 10.1021/ja400701c [PubMed: 23565806]
31. Stover RJ, Murthy AK, Nie GD, Gourisankar S, Dear BJ, Truskett TM, Sokolov KV, Johnston KP. Quenched assembly of nir-active gold nanoclusters capped with strongly bound ligands by tuning particle charge via ph and salinity. J Chem Phys C. 2014; 118(26):14291–14298. arXiv:http://dx.doi.org/10.1021/jp408715p. DOI: 10.1021/jp408715p
32. Villarreal O, Chen L, Whetten R, Demeler B. Aspheric solute ions modulate gold nanoparticle interactions in an aqueous solution: An optimal way to reversibly concentrate functionalized nanoparticles. J Phys Chem B. 2015; 119(50):15502–15508. DOI: 10.1021/acs.jpcb.5b09864 [PubMed: 26581232]
33. Jadzinsky PD, Calero G, Ackerson CJ, Bushnell DA, Kornberg RD. Structure of a thiol monolayer-protected gold nanoparticle at 1.1 å resolution. Science. 2007; 318(5849):430–433. arXiv:http://www.sciencemag.org/content/318/5849/430.full.pdf. DOI: 10.1126/science.1148624 [PubMed: 17947577]
34. Lopez-Acevedo O, Akola J, Whetten RL, Grönbeck H, Häkkinen H. Structure and bonding in the ubiquitous icosahedral metallic gold cluster au144(sr)60. J Chem Phys C. 2009; 113(13):5035–5038. arXiv:http://dx.doi.org/10.1021/jp8115098. DOI: 10.1021/jp8115098
35. Heikkilä E, Gurtovenko AA, Martinez-Seara H, Häkkinen H, Vattulainen I, Akola J. Atomistic simulations of functional au144(sr)60 gold nanoparticles in aqueous environment. J Chem Phys C. 2012; 116(17):9805–9815. arXiv:http://dx.doi.org/10.1021/jp301094m. DOI: 10.1021/jp301094m
36. Tlahuice-Flores A, Black DM, Bach SBH, Jose-Yacamán M, Whetten RL. Structure & bonding of the gold-subhalide cluster I-Au144Cl60[z]. Phys Chem Chem Phys. 2013; 15:19191.doi: 10.1039/c3cp53902d [PubMed: 24105400]
37. Bahena D, Bhattarai N, Santiago U, Tlahuice A, Ponce A, Bach SBH, Yoon B, Whetten RL, Landman U, Jose-Yacaman M. Stem electron diffraction and high-resolution images used in the determination of the crystal structure of the au144(sr)60 cluster. J Phys Chem Lett. 2013; 4(6): 975–981. arXiv:http://dx.doi.org/10.1021/jz400111d. DOI: 10.1021/jz400111d [PubMed: 23687562]
38. Heikkilä E, Martinez-Seara H, Gurtovenko AA, Vattulainen I, Akola J. Atomistic simulations of anionic au144(sr)60 nanoparticles interacting with asymmetric model lipid membranes. Biochim Biophys Acta. 2014; 1838(11):2852.doi: 10.1016/j.bbamem.2014.07.027 [PubMed: 25109937]
39. Alsharif SA, Chen LY, Tlahuice-Flores A, Whetten RL, Yacaman MJ. Interaction between functionalized gold nanoparticles in physiological saline. Phys Chem Chem Phys. 2014; 16(9): 3909–3913. DOI: 10.1039/C3CP54503B [PubMed: 24441708]
40. Villarreal OD, Chen LY, Whetten RL, Yacaman MJ. Ligand-modulated interactions between charged monolayer-protected au144(sr)60 gold nanoparticles in physiological saline. Phys Chem Chem Phys. 2015; 17(5):3680–8. DOI: 10.1039/c4cp05137h [PubMed: 25556346]
41. Humphrey W, Dalke A, Schulten K. Vmd: Visual molecular dynamics. J Mol Graph. 1996; 14(1): 33–38. DOI: 10.1016/0263-7855(96)00018-5 [PubMed: 8744570]
42. Vanommeslaeghe K, Hatcher E, Acharya C, Kundu S, Zhong S, Shim J, Darian E, Guvench O, Lopes P, Vorobyov I, Mackerell AD. Charmm general force field: A force field for drug-like molecules compatible with the charmm all-atom additive biological force fields. J Comput Chem. 2010; 31(4):671–690. DOI: 10.1002/jcc.21367 [PubMed: 19575467]
43. Jorgensen WL, Chandrasekhar J, Madura JD, Impey RW, Klein ML. Comparison of simple potential functions for simulating liquid water. J Chem Phys. 1983; 79(2):926–935. doi:doi:http://dx.doi.org/10.1063/1.445869.

44. Martyna GJ, Tobias DJ, Klein ML. Constant pressure molecular dynamics algorithms. J Chem Phys. 1994; 101(5):4177–4189. DOI: 10.1063/1.467468
45. Feller SE, Brown CA, Nizza DT, Gawrisch K. Nuclear over-hauser enhancement spectroscopy cross-relaxation rates and ethanol distribution across membranes. Biophys J. 2002; 82(3):1396–1404. doi:http://dx.doi.org/10.1016/S0006-3495(02)75494-5. [PubMed: 11867455]
46. Phillips JC, Braun R, Wang W, Gumbart J, Tajkhorshid E, Villa E, Chipot C, Skeel RD, Kal L, Schulten K. Scalable molecular dynamics with namd. J Comput Chem. 2005; 26(16):1781–1802. DOI: 10.1002/jcc.20289 [PubMed: 16222654]
47. Wong OA, Heinecke CL, Simone AR, Whetten RL, Ackerson CJ. Ligand symmetry-equivalence on thiolate protected gold nanoclusters determined by nmr spectroscopy. Nanoscale. 2012; 4:4099–4102. DOI: 10.1039/C2NR30259D [PubMed: 22543449]
48. Heinecke CL, Ackerson CJ. Preparation of gold nanocluster bioconjugates for electron microscopy. Methods in molecular biology (Clifton, NJ). 2013; 950:293.
49. Deng Y, Roux B. Computations of standard binding free energies with molecular dynamics simulations. J Phys Chem B. 2009; 113(8):2234–46. DOI: 10.1021/jp807701h [PubMed: 19146384]
50. Gambinossi F, Chanana M, Mylon SE, Ferri JK. Stimulus-responsive au@(meo2max-co-oegmay) nanoparticles stabilized by non-dlvo interactions: Implications of ionic strength and copolymer (x:y) fraction on aggregation kinetics. Langmuir. 2014; 30(7):1748–1757. DOI: 10.1021/la403963c [PubMed: 24517439]
51. Grasso D, Subramaniam K, Butkus M, Strevett K, Bergendahl J. A review of non-dlvo interactions in environmental colloidal systems. Rev Environ Sci Biotechnol. 2002; 1(1):17–38. DOI: 10.1023/A:1015146710500
52. Chang Y-I, Chang P-K. The role of hydration force on the stability of the suspension of saccharomyces cerevisiaeapplication of the extended dlvo theory. Colloids Surf, A. 2002; 211(1): 67–77. doi:http://dx.doi.org/10.1016/S0927-7757(02)00238-8.
53. Sousa AA, Hassan SA, Knittel LL, Balbo A, Aronova MA, Brown PH, Schuck P, Leapman RD. Biointeractions of ultrasmall glutathione-coated gold nanoparticles: effect of small size variations. Nanoscale. 2016; 8:6577–6588. DOI: 10.1039/C5NR07642K [PubMed: 26934984]
54. Ho JD, Yeh R, Sandstrom A, Chorny I, Harries WEC, Robbins RA, Miercke LJW, Stroud RM. Crystal structure of human aquaporin 4 at 1.8 angstrom and its mechanism of conductance. Proc Natl Acad Sci U S A. 2009; 106(18):7437–7442. DOI: 10.1073/pnas.0902725106 [PubMed: 19383790]

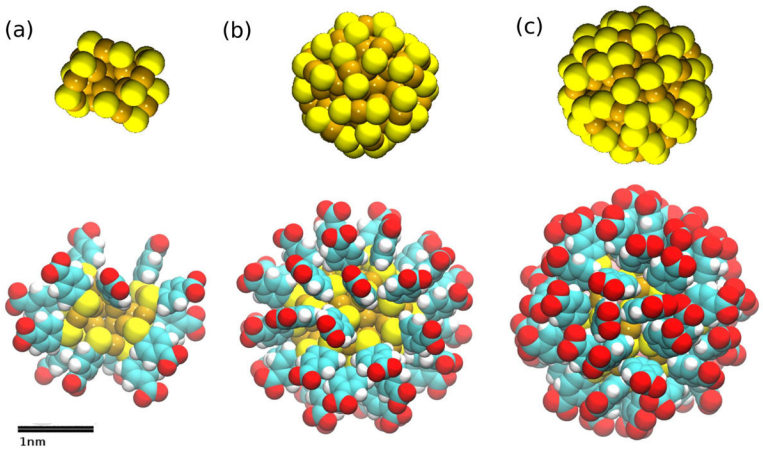

Figure 1.

Systems under study: (a) the $Au_{18}(SR)_{14}$ (diameter ~1nm), (b) $Au_{102}(SR)_{44}$ (diameter ~ 1.5nm) and (c) $Au_{144}(SR)_{60}$ (diameter ~2nm) NPs represented as spheres (with van der Waals radius). The coloring scheme throughout this paper is the following: sulfur, yellow; oxygen, red; carbon, cyan; hydrogen, white; gold, golden; nitrogen, blue. All graphics were rendered with VMD.[41]

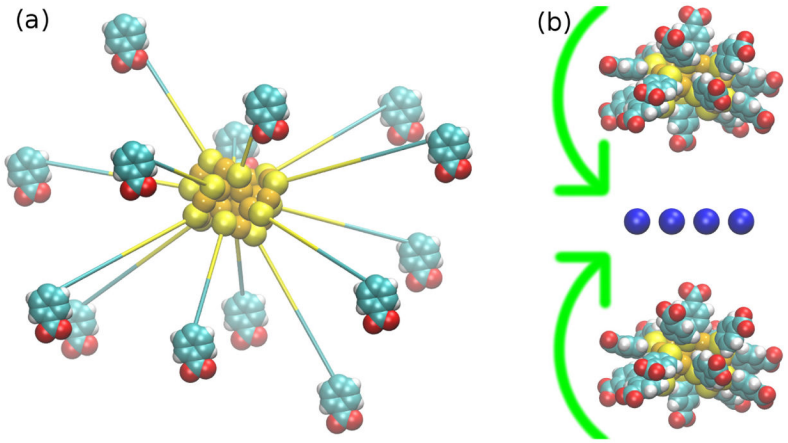

Figure 2.

Building procedure: (a) The Au_{18} NP structure undergoing energy minimization after attaching 14 ligands to its surface. (b) The Au_{18} NP pair undergoing free rotation in the presence of a layer of Na^{+} located at the middle, in order to find the orientation of minimum energy.

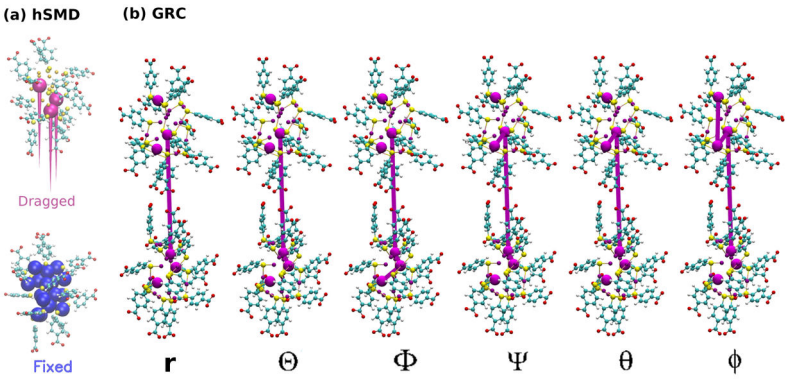

Figure 3.

Methodology for the PMF calculations of Au_{18} (a) *The hSMD method:* The displacements of the 3 pulling gold atoms are shown as magenta cones. (b) *The method of geometrical restraints:* The six groups employed to define the six collective variables are represented as purple spheres. The groups involved in the definition of each collective variable are connected by purple lines.

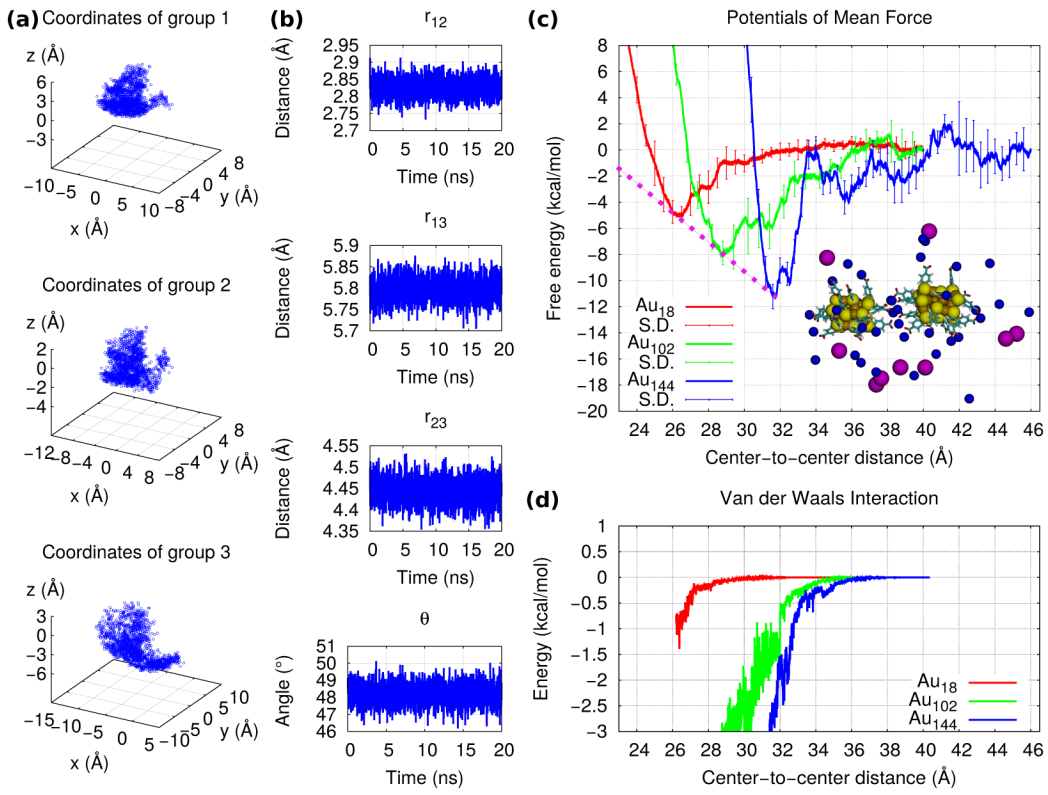

Figure 4.

hSMD results : (a) Histogram of the coordinates of the three Au_{18} pulling atoms during the bound-state equilibration employed to compute Z_0. (b) The distances among the three Au_{18} pulling atoms and the angle formed by them vs. time during the unbound-state equilibration employed to compute Z_∞. (c) The PMFs of Au_{18}, Au_{102} and Au_{144} as functions of distance between the cores' centers of mass. The minima are connected by a dashed pink line. The snapshot shows the bound state of Au_{18} and all ions within 20 Å of the NPs colored by name: sodium, blue; chloride, magenta. (d) The energetic contributions to the PMF from the van der Waals interactions.

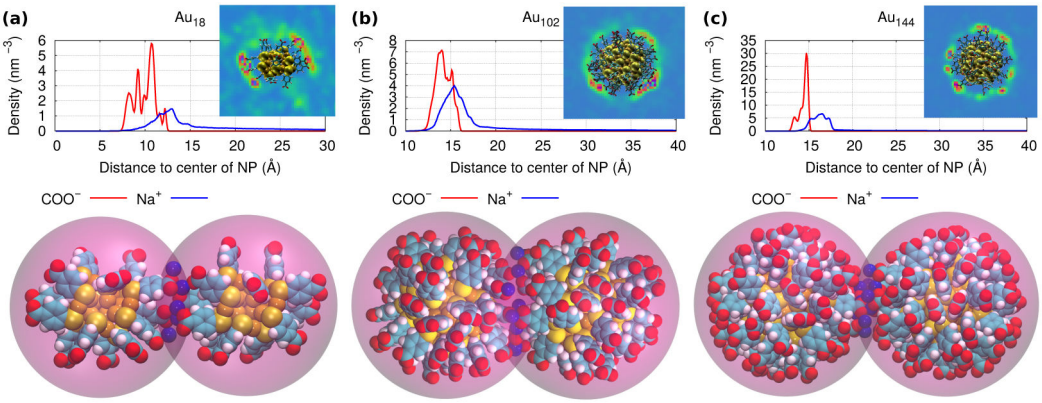

Figure 5.

The radial density distributions of the carboxyl groups and the sodium counterions around (a) $Au_{18}(SR)_{60}$, (b) $Au_{102}(SR)_{44}$ and (c) $Au_{144}(SR)_{60}$. The snapshots on the top show the density maps of sodium around the NP (the coloring scheme in order of increasing density is: blue, green, red). The snapshots at the bottom show the sodium lying within 3.5 Å of both NPs simultaneously at the bound state.

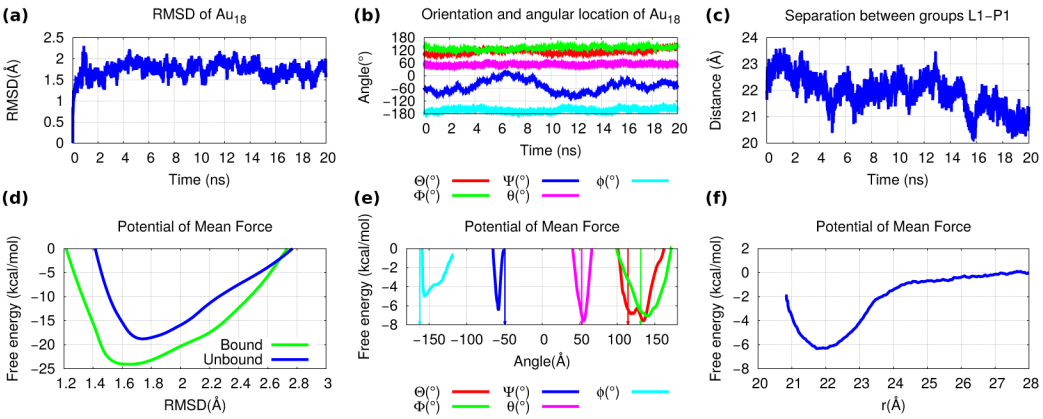

Figure 6.

Geometrical restraint results for Au_{18}: The (a) conformational (i.e. RMSD), (b) angular (i.e. Euler angles for orientation and spherical angles for location) and (c) radial collective variables as functions of time for the 20 ns of simulation under equilibrium conditions. The PMF profiles as functions of the (d) conformational, (e) angular and (f) radial collective variables. The values employed as minima for each of the constraint potentials are indicated by arrows.

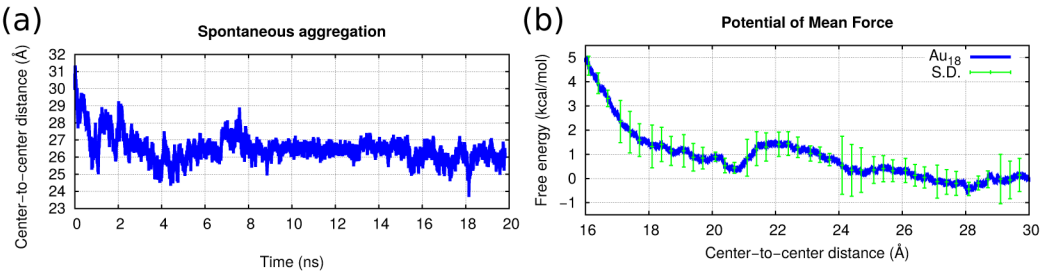

Figure 7.

(a) The center-to-center separation between two free Au_{18} NPs vs. time. Starting with an initial value of 3 nm, their aggregation is spontaneous. (b) The PMF of Au_{18} as a function of the center-to-center separation, employing the opposite orientation as in Fig. 4. The net interaction becomes repulsive.

Table 1

The free energy calculations for the Au18, Au102 and Au144 NPs.

hSMD			
	Au_{18}	**Au_{102}**	**Au_{144}[40]**
Z_0	1.5×10^6		
$\Delta \mathscr{W}_{0,\infty}$ $\left(\frac{kcal}{mol}\right)$	−5.0	−8.2	−11
Z_∞	5.6×10^4		
ΔG_{bind} $\left(\frac{kcal}{mol}\right)$	−2.6	−6.2	−12
$\mathbf{K}_D$	13 mM	30 μM	3.2 nM
Geometrical Restraints (Au_{18})			
ΔG_c^{site} $\left(\frac{kcal}{mol}\right)$	−13	$\Delta G_\phi^{\text{site}}$ $\left(\frac{kcal}{mol}\right)$	−2.3
$\Delta G_\Theta^{\text{site}}$ $\left(\frac{kcal}{mol}\right)$	−1.4	$-k_B T \ln\left(c_0 S^* I^*\right)$ $\left(\frac{kcal}{mol}\right)$	−3.0
$\Delta G_\Phi^{\text{site}}$ $\left(\frac{kcal}{mol}\right)$	−1.0	ΔG_o^{bulk} $\left(\frac{kcal}{mol}\right)$	6.7
$\Delta G_\Psi^{\text{site}}$ $\left(\frac{kcal}{mol}\right)$	−3.5	ΔG_c^{bulk} $\left(\frac{kcal}{mol}\right)$	15.0
$\Delta G_\theta^{\text{site}}$ $\left(\frac{kcal}{mol}\right)$	−0.33	ΔG_{bind} $\left(\frac{kcal}{mol}\right)$	−2.8
$\mathbf{K}_D$	9.0 mM		